RSC Advances

COMMUNICATION

View Article Online
View Journal | View Issue

Cite this: RSC Adv., 2015, 5, 70713

Hierarchical metal nanomesh/microgrid structures for high performance transparent electrodes†

Tongchuan Gao,[a] Po-Shun Huang,[b] Jung-Kun Lee[b] and Paul W. Leu*[a]

Received 27th July 2015
Accepted 10th August 2015

DOI: 10.1039/c5ra14851k

www.rsc.org/advances

We report a comprehensive study on the optical and electronic properties of hierarchical metal nanomesh (NM)/microgrid (MG) structures to determine their performance as transparent conductors (TCs). The NM helps deliver or collect carriers locally while the lower resistance MG transports carriers over larger distances. The structures exhibit high uniformity of optical and electronic properties. Hierarchical Ag NM/Ag MG structures demonstrate 83% diffusive transmission at a sheet resistance of 0.7 Ω per square when fabricated directly on quartz and 81% at 0.7 Ω per square when fabricated directly on flexible plastic. The direct current to optical conductivity ratios σ_{dc}/σ_{op} of these structures are 2900 and 2300, respectively. This corresponds to over an order of magnitude reduction in sheet resistance with a negligible to slight reduction in transmission compared to NMs. The haze factor of these structures may be tuned by modifying the NM hole diameter. Furthermore, the hierarchical structures exhibit good durability under bending and heating.

1 Introduction

Transparent conductors (TCs) are important as the top electrode for a variety of optoelectronic devices, including solar cells, flat panel displays, touch screens, and light-emitting diodes. Currently, indium tin oxide (ITO) films are the most commonly used TC structures,[1] because of their high optical transparency and low electrical resistivity. High quality ITO films have sheet resistance values R_s of about 10 Ω per square (sq) at transmission $T = 85\%$.[2] However, ITO is increasingly expensive, because indium is a rare metal with rising cost[3] and ITO is commercially deposited by dc magnetron sputtering, which has higher cost than chemical vapor deposition (CVD) or vacuum evaporation.[4] Furthermore, ITO is a brittle material and the processing includes annealing at elevated temperature, making it a poor candidate for emerging flexible electronics.

A variety of nanostructured materials have emerged as potential substitutes for ITO and other doped metal oxides, such as percolation networks of metal nanowires (NWs)[5,6] or carbon nanotubes,[7] metal nanomeshes (NMs),[8] nanoparticle wire arrays,[9] graphene-based materials,[2,10,11] and hybrid structures.[12,13] Percolation network films fabricated by solution-based methods and vacuum filtration[7,14] have demonstrated comparable optical transmission and sheet resistance to ITO films.[5,15–17] However, it is desirable to further reduce R_s to minimize the Joule loss in current-driven devices.[18]

For percolation network films, R_s is inherently limited by contact resistance[19] and percolation effects.[20] A variety of post-treatment methods, such as thermal annealing,[15] plasmonic welding,[21] and chemical linking[22] have been studied to reduce the wire–wire contact resistance without much loss in transparency. Metal NW films with larger NW diameters and pitches tend to have better TC performance.[23,24] However, a large separation between NWs will result in poor localized conductivity and thus, poor uniform carrier collection or delivery. This is especially a problem for organic optoelectronic devices, which have short exciton diffusion lengths.[25] Moreover, the percolation effects will be more pronounced due to the sparseness and the randomness of the networks. Conductive polymers have been used to relieve the percolation effect and achieve a smooth surface.[26,27]

Recently, hierarchical structures have been demonstrated for TCs with very low sheet resistance and excellent transparency.[8,18] For example, random Ag NW films have recently been combined with mesoscale wires (widths from 1 to 5 μm) to demonstrate $T = 92\%$ at $R_s = 0.36$ Ω per sq or a σ_{dc}/σ_{op} of over 12 000.[18] The ratio of dc conductivity to optical conductivity σ_{dc}/σ_{op} is a commonly used figure of merit (FoM) for TCs.[28] However, these structures suffer from some of the same contact resistance issues of random NW films and for example, must be annealed at 200 °C for 40 minutes to fuse the different length

[a]Department of Industrial Engineering, University of Pittsburgh, Pittsburgh, PA 15261, USA. E-mail: pleu@pitt.edu

[b]Department of Mechanical Engineering & Materials Science, University of Pittsburgh, Pittsburgh, PA 15261, USA

† Electronic supplementary information (ESI) available: Details of simulation methods; design criterion of the hierarchical Ag NM/MG; and fabrication process of Ag MG. See DOI: 10.1039/c5ra14851k

scale wires. The randomness of the structure may also result in less uniform sheet resistance and optical properties over micron length scales. We have also recently demonstrated a hierarchical structure that integrates high quality graphene grown by CVD with a metal grid to achieve $T = 94\%$ at $R_s = 0.6\ \Omega$ per sq or a σ_{dc}/σ_{op} of almost 9000.[12]

In this paper, we conducted both simulations and experiments to investigate the performance of hierarchical Ag nanomesh (NM)/Ag microgrid (MG) structures as TCs. The hierarchical structure exhibits diffusive transmission $T = 83\%$ at $R_s = 0.7\ \Omega$ per sq or $\sigma_{dc}/\sigma_{op} = 2900$ when fabricated on a quartz substrate and $T = 81\%$ at $R_s = 0.7\ \Omega$ per sq or $\sigma_{dc}/\sigma_{op} = 2300$ when fabricated on a polyethylene terephthalate (PET) substrate. In contrast, Ag NMs fabricated on quartz exhibit $T = 83\%$ at $R_s = 13\ \Omega$ per sq or $\sigma_{dc}/\sigma_{op} = 140$. The sheet resistance of the NM may be decreased by over an order of magnitude with only a slight decrease in transmission by integration with the MG. The hierarchical structures also exhibit more uniform resistance and optical properties on the microscale compared with random networks of nanowires. We demonstrate the tunability of haze factor in our NM/MG structures, which is important for various optoelectronic applications. In addition, we performed durability experiments to assess the performance of the Ag NM/MG under various bending and heating conditions.

2 Results and discussion

Fig. 1(a) shows a schematic of the hierarchical NM/MG structure. The Ag NM consists of a hexagonal array of holes in a Ag thin film. The primitive lattice vectors are $\vec{a_1}$ and $\vec{a_2}$ with $\left|\vec{a_1}\right| = \left|\vec{a_2}\right| = a_{NM}$. The NM is fabricated using a microsphere lithography approach, which we have previously reported for Cu.[8] A 50 nm thick SiO_2 film is coated on PET substrates to protect the substrate from being etched in the reactive ion etching (RIE) process. The method is scalable and has been demonstrated on 1 m^2 glass substrates.[29] Specific control over the various NM geometric parameters, pitch a_{NM}, thickness t_{NM}, and width w_{NM}, may be accomplished through variation in the self-assembly of microspheres or nanospheres,[30] etching time, and metal evaporation time. The geometric parameters for the MG include the pitch a_{MG}, width w_{MG}, and thickness t_{MG}. The Ag MG is fabricated by photolithography with lift-off metal patterning. Please refer to ESI† for details. Fig. 1(b) shows representative scanning electron microscope (SEM) images of the Ag NM/MG structure with $a_{NM} = 2000$ nm, $w_{NM} = 100$ nm, and $t_{NM} = 30$ nm, and $a_{MG} = 500\ \mu$m, $w_{MG} = 10\ \mu$m, and $t_{MG} = 1\ \mu$m. The high uniformity and long-range order of the structure is apparent in the images, where these qualities address the percolation and contact resistance issues of random nanowire networks or disordered structures. Fig. 1(c) shows atomic force microscope (AFM) images of the structure. Smooth Ag surfaces for both MG and NM are observed in the height profile and the

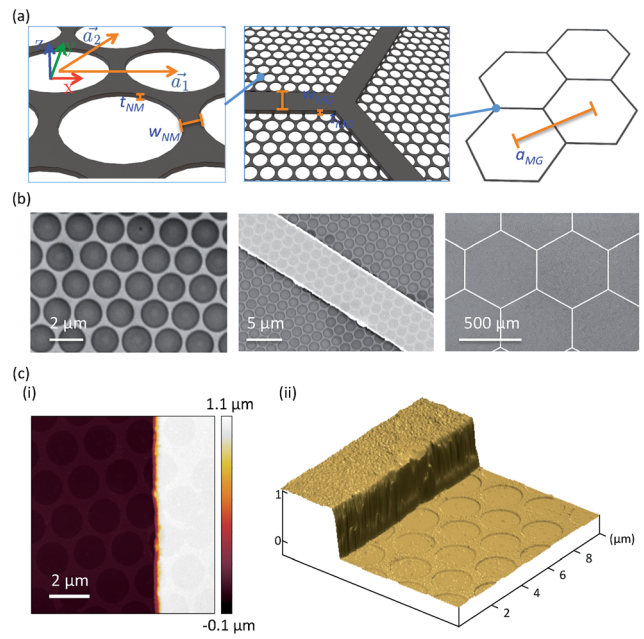

Fig. 1 (a) Schematic of the hierarchical Ag NM/MG structure and various geometric parameters that define its morphology. (b) SEM images of Ag NM/MG structure at different magnifications. (c) AFM images of Ag NM/MG structure for (i) height profile and (ii) 3D topography. The geometric parameters are $a_{NM} = 2000$ nm, $w_{NM} = 100$ nm, $t_{NM} = 30$ nm, and $a_{MG} = 500\ \mu$m, $w_{MG} = 10\ \mu$m, and $t_{MG} = 1\ \mu$m.

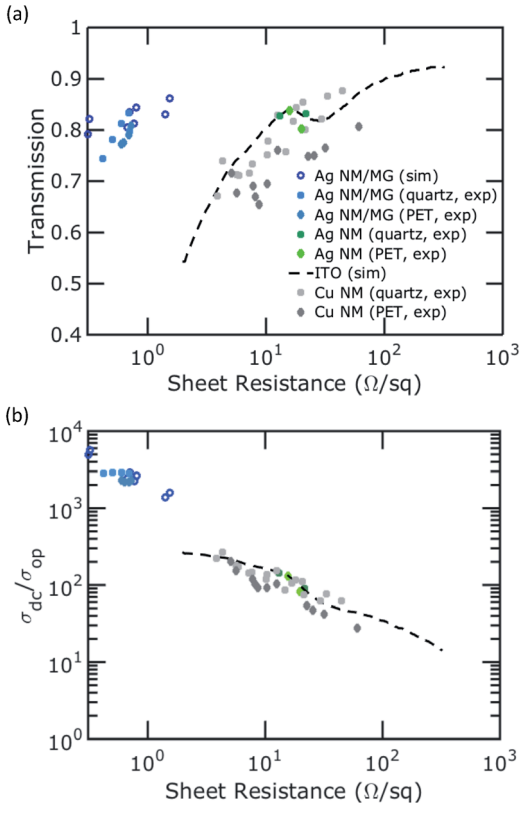

Fig. 2 (a) Transmission *versus* sheet resistance for TCs. Our Ag NM/MG data is shown in shades of blue and NM data is shown in shades of green at $\lambda = 550$ nm. Data for Cu NMs on quartz and PET substrates[8] and simulated ITO thin films[15] is also shown. (b) FoM *versus* sheet resistance for the same data.

3D topography. The color bar in Fig. 1(c)(i) is intentionally set to start from −0.1 μm to improve the contrast.

Fig. 2(a) plots the relationship between diffusive transmission and sheet resistance for the hierarchical NM/MG structures along with various other TCs in the literature. The data for Ag NM/MG structures are plotted with various shades of blue for simulations and experiments on quartz and PET substrates. Experimentally fabricated Ag NM data on quartz and PET substrates are plotted with different shades of green. Our transmission data are plotted at the wavelength $\lambda = 550$ nm, which is near the middle of the visible spectrum. The effect of the substrates has been excluded. For comparison purposes, we plot simulation data for ITO thin films[15] as well as our previously reported Cu NMs on quartz and PET substrates.[8]

Ag NMs exhibit comparable performance to ITO thin films and Cu NMs. The Ag NMs exhibit similar performance to Cu NMs because the transmission properties at the length scales involved are primarily independent of the material, and the resistivity of Ag is close to that of Cu.[23,24] The Ag NMs fabricated on rigid quartz performs slightly better than that fabricated on PET due to the better uniformity and ordering of the structure.[8] The R_s of the Ag NMs is between 13 and 21 Ω per sq with about 83% transmission on quartz, and on PET, R_s is between 16 and 20 Ω per sq with a transmission between 81% and 83%. By integrating the Ag NM with the MG, the sheet resistance may be decreased substantially by over an order of magnitude without significant decrease in transmission. The R_s of the hierarchical Ag NM/MG on quartz is between 0.4 and 0.7 Ω per sq with a transmission between 74% and 83% and on PET is between 0.6 and 0.7 Ω per sq with a transmission between 77% and 81%. Our data demonstrates that Ag NM/MG samples fabricated on quartz substrates or PET substrates exhibit superior performance to ITO films. The FoM σ_{dc}/σ_{op} can be represented in terms of T and R_s by $T = \left(1 + \frac{Z_0}{2R_s}\frac{\sigma_{op}}{\sigma_{dc}}\right)^{-2}$, where $Z_0 = 377$ Ω is the free space impedance. The Ag NM has a σ_{dc}/σ_{op} of between 80 and 140. However, typical industry requirements are $\sigma_{dc}/\sigma_{op} = 350$.[2] Fig. 2(b) plots the FoM σ_{dc}/σ_{op} of these TCs *versus* sheet resistance. By integrating the NM with the MG, we can improve σ_{dc}/σ_{op} drastically to over 2000.

Fig. 3(a) plots both the simulated and experimentally measured (on quartz) diffusive transmission spectrum for the hierarchical structure with $a_{NM} = 2000$ nm, $w_{NM} = 100$ nm, $t_{NM} = 30$ nm, $a_{MG} = 200$ μm, $w_{MG} = 5$ μm, and $t_{MG} = 1$ μm. The simulated and experimental transmission spectra are reasonably close to each other, where the minor differences can be accounted for by statistical variations and imperfections in the fabricated structure. The simulated R_s for this geometry is 0.67 Ω per sq while the measured R_s was 0.70 Ω per sq. The haze factor, defined as $\frac{T - T_{spec}}{T}$, is an important property for transparent conductors, where T is the diffusive transmission and

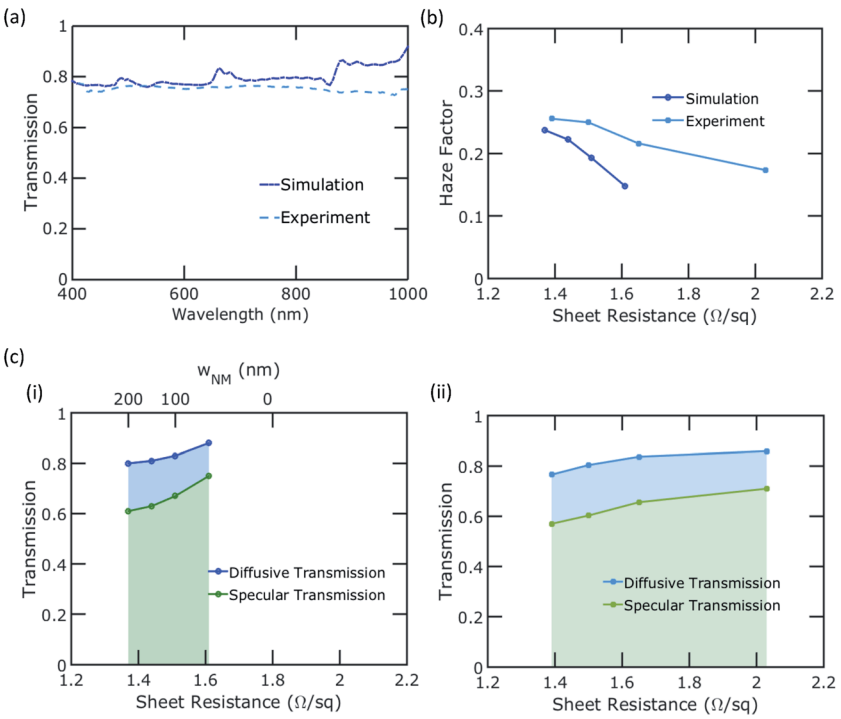

Fig. 3 (a) Diffusive transmission spectrum for Ag NM/MG with $a_{NM} = 2000$ nm, $w_{NM} = 100$ nm, $t_{NM} = 30$ nm, $a_{MG} = 200$ μm, $w_{MG} = 5$ μm, and $t_{MG} = 1$ μm obtained by simulation and experiment. (b) Haze factor as a function of sheet resistance for experimental and simulated samples with $a_{MG} = 500$ μm, $w_{MG} = 5$ μm, $t_{MG} = 1$ μm, $a_{NM} = 2000$ nm, $t_{NM} = 20$ nm, and various w_{NM}. (c) Diffusive transmission and specular transmission as a function of sheet resistance at $\lambda = 550$ nm for Ag NM/MG with different extends of haziness using (i) simulation and (ii) experiment. w_{NM} is varied from 200 to 50 nm in simulation to match the experimental geometry and is labelled accordingly. $w_{NM} = 0$ corresponds to that the sheet resistance is only contributed by Ag MG.

T_{spec} is the specular transmission.[31] The haze factor of the hierarchical metal NM/MG transparent conductors is tunable by changing the geometric parameters and materials. The haze factor is mostly determined by diffraction and scattering from the NM, because its dimensions are of the same magnitude as the wavelength of incident light. The MG only introduces a geometric shadow because its features are larger than the wavelengths involved. We investigated the haze factor for Ag NM/MGs with geometric parameters $a_{MG} = 500$ μm, $w_{MG} = 5$ μm, $t_{MG} = 1$ μm, $a_{NM} = 2000$ nm, $t_{NM} = 20$ nm, and various w_{NM} using both simulation and experiments. Fig. 3(c) shows (i) the simulated and (ii) the experimentally measured diffusive and specular transmission *versus* sheet resistance for Ag NM/MGs on quartz. In the simulation, w_{NM} ranges from 50 nm to 200 nm to match the experimental geometry. The haze factor of experimentally fabricated Ag NM/MGs demonstrate the same overall trends as the simulated data, but the haze factor is higher than the simulation results due to imperfections in the surfaces and NM periodicity. The simulated haze factor increases from 8% to 15% as w_{NM} increases from 50 nm to 200 nm, while R_s decreases from 1.6 to 1.4 Ω per sq. The haze factor in the fabricated samples increases from 17% to 26%, while R_s decreases from 2.0 to 1.4 Ω per sq correspondingly. The haze factor of the NM/MG can be tuned while maintaining a low sheet resistance because the overall conductance of the NM/MG is primarily due to the MG. As the NM width increases, the hole diameter decreases and the Airy pattern from Fraunhofer diffraction broadens.[32] This results in a higher fraction of photons transmitted at nonnormal angles. The tunability of haze factor is important for solar cells because a high haze factor is desirable for increasing the coupling of light into the absorber.

Lastly, various durability tests were performed to evaluate the robustness of the Ag NM/MG in applications. Fig. 4(a) shows the variation in the resistance of two Ag NM/MG samples on PET substrates after both bending in compression and tension. Two Au contacts were deposited on the samples using an e-beam evaporator, and the resistance between the two contacts was monitored after bending. The samples were bent around a steel rod with 1 cm diameter with the structure toward and away from the rod for compression and tension tests, respectively. The samples for both bending tests have a geometry of $a_{NM} = 2000$ nm, and $w_{NM} = 100$ nm, $t_{NM} = 30$ nm, $a_{MG} = 500$ μm, $w_{MG} = 10$ μm, and $t_{MG} = 1$ μm. The original resistance of the samples prepared for the tension and compression tests are 4.3 Ω per sq and 4.0 Ω per sq, respectively. After 200 cycles of bending, the resistance of the samples are 6.1 Ω per sq and 5.3 Ω per sq, corresponding to a 39.5% and 32.5% increase, respectively. The degradation of the sample is mainly due to the delamination of the Ag MG from the SiO_2 coated PET substrate, as shown in Fig. 4(b)(i). The Ag NM, which is more resilient under bending,[8] is mostly intact after the bending test, as shown in Fig. 4(b)(ii). In locations where the MG has delaminated, the underlying NM is also removed, suggesting a strong mechanical connection between the two metal layers.

Fig. 4(c) shows the change in resistance of a Ag NM/MG on PET substrate after the heating test. The sample morphology is $a_{NM} = 2000$ nm, $w_{NM} = 150$ nm, $t_{NM} = 30$ nm, $a_{MG} = 500$ μm, $w_{MG} = 10$ μm, and $t_{MG} = 1$ μm. After continuous heating for 168 hours (h) on a hot plate at 65 °C, the resistance of the sample changed from 2.0 to 2.7 Ω per sq, increasing by 35%. Ag is prone to oxidation and passivation of the sample may help reduce sheet resistance degradation, especially at higher temperatures.[33]

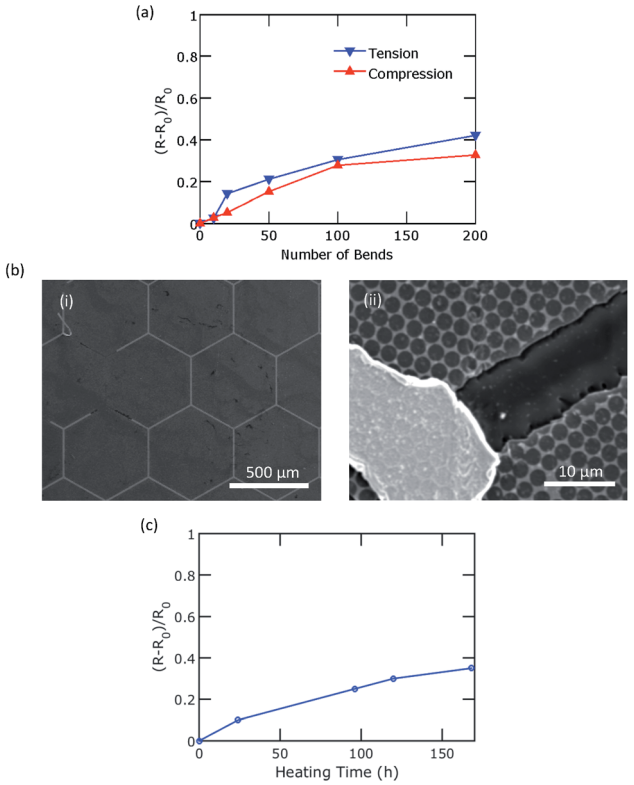

Fig. 4 Durability tests for Ag NM/MG on PET substrates. (a) Resistance change *versus* number of bends for Ag NM/MG on PET substrates. The bending curvature is 0.5 cm. (b) SEM image for the sample after bending test. (c) Resistance change *versus* heating time for Ag NM/MG on PET substrate heated at 65 °C in air.

3 Conclusions

In conclusion, we reported both simulations and experiments on the optical and electrical properties hierarchical Ag NM/MG structures for TCs. Simulations compare reasonably to experimental results and can be used to guide the design of the hierarchical structures. Experimentally, we demonstrate a scalable method to fabricate Ag NM/MG on both rigid quartz substrates and flexible PET substrates. The samples demonstrate good uniformity and ordering, with superior performance to ITO. The haze factor of the hierarchical structure for TCs can be tuned to suit the requirements for different applications. Durability tests demonstrate that the hierarchical structures are not significantly sensitive to bending and heating.

Acknowledgements

This work was supported in part by NSF grant #1233151. Computing resources were provided by the Center for

Simulation and Modeling at the University of Pittsburgh. The authors would also like to thank the Mascaro Center for Sustainable Innovation for support. J.-K. Lee's portion was supported by the Global Frontier R & D Program on Center for Multiscale Energy System funded by the National Research Foundation, Korea (2012M3A6A7054855).

References

1 C. G. Granqvist and A. Hultåker, *Thin Solid Films*, 2002, **411**, 1–5.
2 S. De and J. N. Coleman, *ACS Nano*, 2010, **4**, 2713–2720.
3 T. Minami, *Thin Solid Films*, 2008, **516**, 5822–5828.
4 R. G. Gordon, *MRS Bull.*, 2000, **25**, 52–57.
5 S. De, T. M. Higgins, P. E. Lyons, E. M. Doherty, P. N. Nirmalraj, W. J. Blau, J. J. Boland and J. N. Coleman, *ACS Nano*, 2009, **3**, 1767–1774.
6 A. R. Rathmell and B. J. Wiley, *Adv. Mater.*, 2011, **23**, 4798–4803.
7 L. Hu, D. S. Hecht and G. Grüner, *Nano Lett.*, 2004, **4**, 2513–2517.
8 T. Gao, B. Wang, B. Ding, J.-K. Lee and P. W. Leu, *Nano Lett.*, 2014, **14**, 2105–2110.
9 D. Y. Choi, Y. S. Oh, D. Han, S. Yoo, H. J. Sung and S. S. Kim, *Adv. Funct. Mater.*, 2015, **25**, 3888–3898.
10 H. Tien, Y. Huang, S. Yang, J. Wang and C. M. Ma, *Carbon*, 2011, **49**, 1550–1560.
11 S. Bae, H. Kim, Y. Lee, X. Xu, J. Park, Y. Zheng, J. Balakrishnan, T. Lei, H. R. Kim, Y. I. Song, Y. Kim, K. S. Kim, B. Ozyilmaz, J. Ahn, B. H. Hong and S. Iijima, *Nat. Nanotechnol.*, 2010, **5**, 574–578.
12 T. Gao, Z. Li, P.-S. Huang, G. J. Shenoy, D. Parobek, S. Tan, J. kun Lee, H. Liu and P. W. Leu, *ACS Nano*, 2015, **9**, 5440–5446.
13 Q. Xu, T. Song, W. Cui, Y. Liu, W. Xu, S.-T. Lee and B. Sun, *ACS Appl. Mater. Interfaces*, 2015, **7**, 3272–3279.
14 H. Koga, M. Nogi, N. Komoda, T. T. Nge, T. Sugahara and K. Suganuma, *NPG Asia Mater.*, 2014, **6**, e93.
15 J. Lee, S. T. Connor, Y. Cui and P. Peumans, *Nano Lett.*, 2008, **8**, 689–692.
16 L. Hu, H. S. Kim, J. Lee, P. Peumans and Y. Cui, *ACS Nano*, 2010, **4**, 2955–2963.
17 J. Lee, P. Lee, H. Lee, D. Lee, S. S. Lee and S. H. Ko, *Nanoscale*, 2012, **4**, 6408–6414.
18 P.-C. Hsu, S. Wang, H. Wu, V. K. Narasimhan, D. Kong, H. Ryoung Lee and Y. Cui, *Nat. Commun.*, 2013, **4**, 2522.
19 H. H. Khaligh and I. A. Goldthorpe, *Nanoscale Res. Lett.*, 2013, **8**, 235.
20 S. De and J. N. Coleman, *MRS Bull.*, 2011, **36**, 774–781.
21 E. C. Garnett, W. Cai, J. J. Cha, F. Mahmood, S. T. Connor, M. Greyson Christoforo, Y. Cui, M. D. McGehee and M. L. Brongersma, *Nat. Mater.*, 2012, **11**, 241–249.
22 Y.-J. Shiau, K.-M. Chiang and H.-W. Lin, *Nanoscale*, 2015, **7**, 12698–12705.
23 T. Gao and P. W. Leu, *Opt. Express*, 2013, **21**, A419.
24 T. Gao and P. W. Leu, *J. Appl. Phys.*, 2013, **114**, 063107.
25 S. Günes, H. Neugebauer and N. S. Sariciftci, *Chem. Rev.*, 2007, **107**, 1324–1338.
26 W. Gaynor, G. F. Burkhard, M. D. McGehee and P. Peumans, *Adv. Mater.*, 2011, **23**, 2905–2910.
27 D. Y. Choi, H. W. Kang, H. J. Sung and S. S. Kim, *Nanoscale*, 2013, **5**, 977–983.
28 M. Dressel and G. Grüner, *Electrodynamics of Solids: Optical Properties of Electrons in Matter*, Cambridge University Press, 1st edn, 2002.
29 P. Gao, J. He, S. Zhou, X. Yang, S. Li, J. Sheng, D. Wang, T. Yu, J. Ye and Y. Cui, *Nano Lett.*, 2015, **15**, 4591–4598.
30 J. Yu, C. Geng, L. Zheng, Z. Ma, T. Tan, X. Wang, Q. Yan and D. Shen, *Langmuir*, 2012, **28**, 12681–12689.
31 D. Langley, G. Giusti, C. Mayousse, C. Celle, D. Bellet and J.-P. Simonato, *Nanotechnology*, 2013, **24**, 452001.
32 M. Born and E. Wolf, *Principles of optics: electromagnetic theory of propagation, interference and diffraction of light*, Cambridge university press, 1999.
33 Y. Ahn, Y. Jeong and Y. Lee, *ACS Appl. Mater. Interfaces*, 2012, **4**, 6410–6414.